




Strength of ceramic–metal joints measured in planar impact experiments

S. Hayun¹, E. Ionash¹, S. Kalabukhov¹, N. Frage¹, and E. Zaretsky^{2,*} 

¹Department of Materials Engineering, Ben-Gurion University of the Negev, P. O. Box 653, 84105 Beer-Sheva, Israel

²Department of Mechanical Engineering, Ben-Gurion University of the Negev, P. O. Box 653, 84105 Beer-Sheva, Israel

Received: 5 September 2017

Accepted: 15 February 2018

Published online:

20 February 2018

© Springer Science+Business Media, LLC, part of Springer Nature 2018

ABSTRACT

SPS-processed alumina and reaction-bonded boron carbide ceramic composite (RBBC) were joined with Al10SiMg alloy by spark plasma sintering and tested in a series of planar impact experiments designed to measure dynamic tensile (spall) strength of the joints. The results of the impact testing, together with postmortem inspection of the fractured samples, confirmed the applicability of this approach for testing joint strength. The measurements show that in the case of an RBBC/metal joint, the dynamic tensile strength of the joint exceeds that of the ceramic part, and that fracture of the shock-loaded ceramic–metal pair occurred in the ceramic portion. The dynamic tensile strength of the interface between alumina and Al10SiMg alloy virtually coincides with that of the metal part, with the fracture occurring exactly at the interface. The coincidence may be explained based on the recently published results of atomistic calculations of the structure of an alumina–aluminum interface.

Introduction

The formation of ceramic–metal joints is a key technology for the use of advanced ceramics in complex structures. The quality of such joints, specifically of the ceramic–metal interface, is responsible for joint reliability. Several methods of joining, such as brazing, thermal spraying, diffusion bonding, and co-sintering, have been developed over the years [1, 2]. Spark plasma sintering (SPS) has been successfully applied for diffusion joining of similar and dissimilar materials [3–9]. In addition to the technological challenges associated with joining, major challenges in characterizing the morphology, composition and

strengths of the interfaces produced remain to be overcome. The morphology and composition of joint regions can be investigated using optical and scanning (SEM) or transmission (TEM) electron microscopy, respectively. At the same time, testing joint strength cannot rely on routine quasi-static methods, which imply that the same stress acts in all cross sections of the tested sample. In such a situation, the sample would fail at its weakest cross section, independently of where this cross section is located. Moreover, in the case of joining two plates of two different materials, such quasi-static testing (for example, in tension) is hardly possible, due to the difficulties in sample preparation.

Address correspondence to E-mail: zheka@bgu.ac.il

We presently suggest that a joint region could be tested by an approach based on the interaction of weak shock waves generated in a tested sample by a planar impact of controlled strength. Such a test could be designed in a manner that would allow application of tensile stress of an a priori estimated amplitude to the joint interface between two materials and not to the materials themselves. A similar technique was used for measuring the adhesive strength of thin turbine blade coating [10]. The method being proposed here is aimed at measuring the strength of the joint between the metallic and ceramic parts of the joined pair without exact knowledge of the location of the joint region. As such, the present paper pursues two objectives, namely to demonstrate the possibility of generating a metal–ceramic joint using Spark Plasma Sintering (SPS) and to demonstrate the simplicity and robustness of the suggested approach for dynamic testing of joint strength.

Experimental

Materials

SPS-processed alumina and reaction-bonded boron carbide infiltrated by silicon (RBBC) were joined with Al10SiMg pre-alloyed powder by SPS. The chemical composition of AlSi10Mg powder, determined by energy-dispersive spectroscopy (EDS), was 89.8 and 10.2 wt.% for aluminum and silicon, respectively. Magnesium content, measured by the Inductively Coupled Plasma (ICP) spectroscopy method, was about 0.4 wt.%.

Alumina powder (Ceralox, high purity SPA-0.5) was inserted into a graphite die/punch set-up (inner diameter 20 mm, outer diameter 40 mm). The die was covered with 20-mm-thick graphite wool to improve thermal insulation. The die was placed in an SPS apparatus (HP D5/1, FCT System, Rauenstein, Germany) equipped with a 50 kN uniaxial press. The sintering procedure was conducted under 1.3 mbar vacuum at 1300 °C. Sixty MPa uniaxial pressure was applied. The heating rate was 25 °C/min, and the holding time at the highest temperatures was 30 min. Microstructural features and mechanical properties of the SPS-processed alumina have been discussed elsewhere [11].

Ceramic preforms (20 mm diameter, 4 mm height) of boron carbide were fabricated from multimodal boron carbide powders [12], which allowed 20 vol.% porosity after uniaxial compaction (180 MPa). Preforms were infiltrated with molten silicon at 1480 °C under a vacuum of $\sim 10^{-4}$ Torr for 20 min.

Joining procedure

Ceramic parts (~ 20 mm diameter) were ground to a thickness of about 3 mm and to a plane parallelism of opposite surfaces of about 0.5 mrad. The surfaces of the ground samples underwent conventional metallographic finishing with 1 μm diamond paste and were then ultrasonically cleaned in hot (60 °C) acetone and dried in air. The ceramic parts, together with about 1.2 g of metal powder, were placed in a graphite die with 20 mm inner and 50 mm outer diameters. The amount of metal powder was chosen to provide a metal part 1.3–1.5 mm-thick in a joint. The bonding process was carried out at 525 °C for 15 min under vacuum (10^{-2} Torr), uniaxial pressure (35 MPa), and a pulsed (5 ms pulse, 2 ms pause) electrical current. In addition, samples from Al10SiMg powder were fabricated using the same SPS parameters.

Microstructure characterization

Microstructural analysis of the ceramics, joint regions, metallic samples and metal parts of ceramic/metal sandwiches recovered after spall experiments was conducted by scanning electron microscopy (SEM, JEOL-35, equipped with a Noran energy-dispersive spectrometer). Metallographic examination was performed after a standard procedure that included cutting the sample along the cross section of interest, grinding and polishing with 1 μm diamond paste. Mechanical characterization of both the ceramic and metal parts is described in “[Determination of the spall strengths of the constituents](#)” section.

Dynamic testing

The joined samples were tested in a series of VISAR-instrumented (Velocity Interferometer System for Any Reflector, [13]) planar impact tests.

Measuring the dynamic tensile (spall) strength of condensed media in planar impact experiments was

based on an analysis of collision of two release waves appearing in the tested material as result of reflection of impact-generated compressive waves from the free surfaces of an impactor and a sample [14]. A simplified (symmetric impact, single wave propagation velocity) scheme of such a collision is shown in Lagrangian coordinates in Fig. 1a. At the time instance $t = 0$, two compressive waves start to travel, one to the right, toward the sample free surface, and the other to the impactor rear surface (for simplicity, it is assumed that both are made of the same material). After reflection from the rear surfaces (of both the sample and impactor), the waves travel in opposite directions, now as release (unloading) waves. Collision of these waves (at a time t_{sp}) results in generating a tensile pulse with amplitude σ_{tens} at the point h_{sp} , as shown in Fig. 1b. If the tensile strength of the sample σ_{sp} is smaller than σ_{tens} , the sample is spall-fractured, with the creation of two new surfaces parallel to the surfaces of the sample and impactor.

As a result, a part of the impact-generated momentum is arrested within the right part of the sample termed the spall plate and reverberated within the plate, causing its periodic compression and tension (states 1-2-3-4 in Fig. 1a, b), expressed in oscillations of the velocity of the free surface of the sample (now, the spall plate). The difference between the first maximum u_{max} and the following minimum u_{min} , known as the velocity pullback

$\Delta u_{sp} = u_{max} - u_{min}$, is related to the spall strength of the sample by $\sigma_{sp} = \rho_0 c^* \Delta u_{sp} / 2$, where ρ_0 is the initial sample density, c^* is some velocity between the longitudinal c_l and bulk c_b speeds of sound [14]. The period of reverberations Δt_{sp} (Fig. 1b) of the velocity of the free surface of the spall plate is related to its thickness by $\Delta h_{sp} = \Delta t_{sp} c_l / 2$. In the case of a routine spall experiment, $\Delta h_{sp} \approx \delta$, where δ is the thickness of the impactor plate.

A similar scheme with some modifications can be applied to evaluate the strength of a joint between two different materials. A scheme of such testing is shown in Fig. 2.

If the tensile pulse amplitude σ_{tens} is lower than the spall strength σ_{sp-r} of the right (with respect to joint) material layer, fracture does not occur at the front part of the pulse. The pulse starts to propagate to the left from the site of a might-have-been spall, finally arriving at the site of the joint between the two materials. If the joint strength σ_j is lower than σ_{tens} , the joint will be disrupted, two new surfaces will be created at the joint site, and the compressive/tensile pulse whose amplitude is determined by the residuary momentum, after fracture of the joint, will reverberate in the right material plate with the period $\Delta t = 2\delta_r / c_{l-r}$, where δ_r and c_{l-r} are, respectively, the thickness of the spall plate and the longitudinal sound speed in the right material. The alternative scenario, $\sigma_j > \sigma_{tens}$, will lead to penetration of the tensile pulse into the left plate and will result in

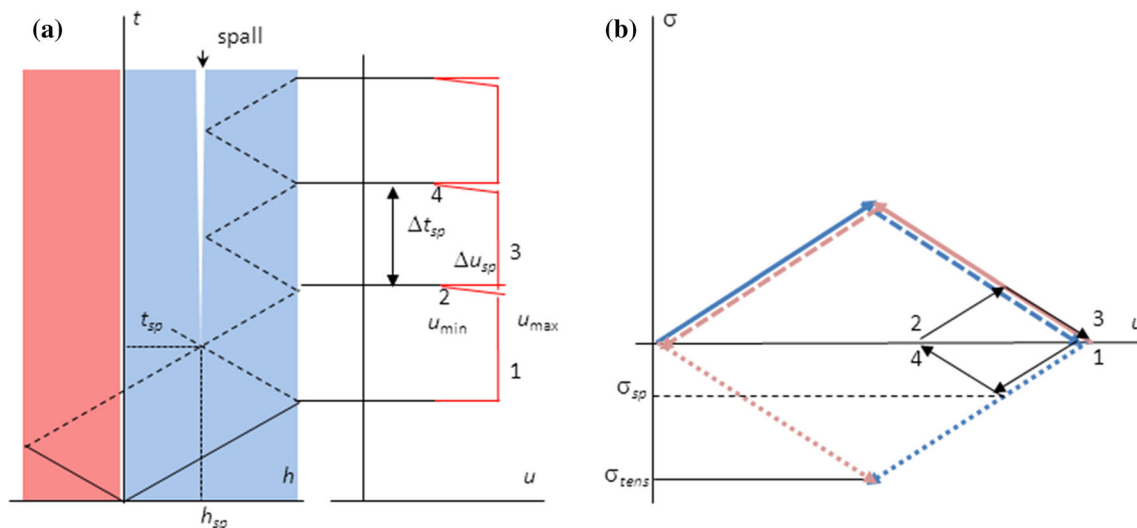


Figure 1 Time t –distance h –free surface velocity u (a), and stress–particle velocity u (b) diagrams of a spall test. The pink and blue areas correspond to the impactor and sample, respectively. In

b, solid lines correspond to loading, dashed lines to unloading, and dotted lines to development of the tensile stress, all with corresponding colors.

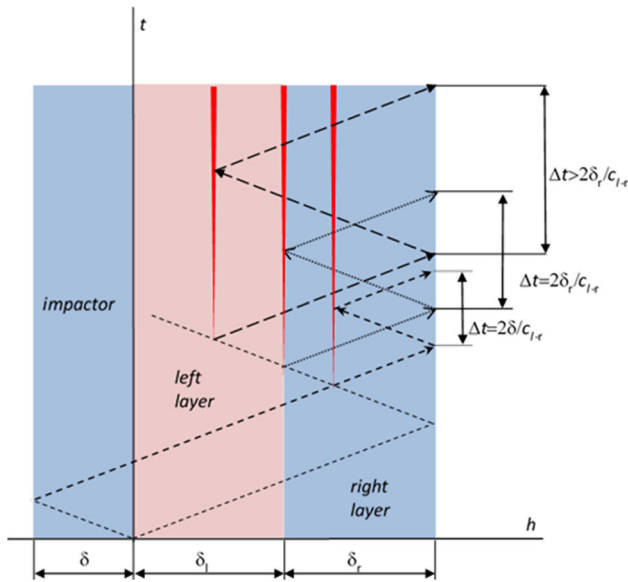
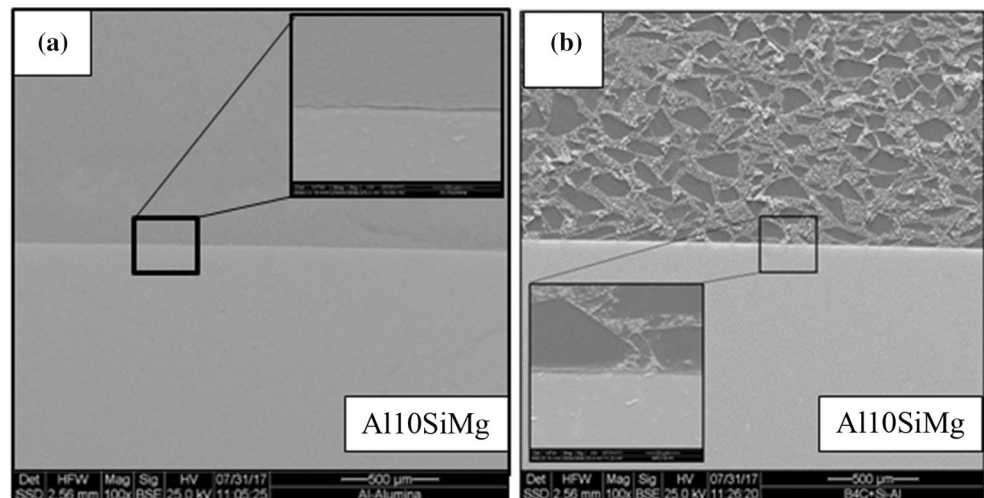


Figure 2 Scheme for testing the joint between two layers of different materials. Dashed lines show the paths of the waves. Different dashing with different arrow heads correspond to signal reverberations after spall (narrow triangles) within the right layer, at the joint, and within the left layer, respectively.

either its spalling ($\sigma_{sp-1} < \sigma_{tens}$) or non-spalling ($\sigma_{sp-1} > \sigma_{tens}$). In the former case, the residual momentum will reverberate between the spall site in the left material layer and the free surface of the right material layer, with a period greater than $\Delta t = 2\delta_r/c_{l-r}$. Combining the spall strength data with the period of the spall signal reverberation allows one to conclude at which tensile stress and at which point the two-layer structure was fractured.

Figure 3 SEM images of $\text{Al}_2\text{O}_3/\text{Al10SiMg}$ (a) and RBBC/ Al10SiMg (b) interfaces. The insets show the joint interfaces with higher magnification.



Results and discussion

Ceramic–metal joint interfaces

Typical SEM images of SPS-processed joints between Al10SiMg and ceramics (Al_2O_3 and RBBC) are presented in Fig. 3. The interfaces were found to be clean and without either voids or discontinuous segments.

Determination of the spall strengths of the constituents

Using the routine spall-oriented loading scheme described in “Dynamic testing” section, the spall strengths σ_{sp} of all the constituents destined for SPS joining, namely sintered Al10SiMg , SPS alumina and RBBC parts, were determined. Prior to spall testing, 20 mm diameter 2 to 4.7 mm-thick plane-parallel samples (ground to 0.5 mrad parallelism) of all three materials were prepared and their longitudinal c_l and shear c_s speeds of sound were measured using the pulse-echo technique. The densities ρ_0 of the samples were determined using the Archimedes method. The results of such examinations, including the values of the bulk speed of sound $c_b = (c_l^2 - 4c_s^2/3)^{0.5}$, longitudinal $E' = \rho_0 c_l^2$, shear $G = \rho_0 c_s^2$, bulk $B = \rho_0 c_b^2$, Young $E = 2(1 + \nu)G$ moduli, and Poisson’s ratio ν , are listed in Table 1.

The uncertainties of determination of ρ_0 , c_l and c_s are mainly standard deviations after ten measurements on one sample. The uncertainties of the rest material parameters, calculated based on these three, are obtained by standard procedure. The uncertainty of the spall strength is caused mainly by uncertainty

Table 1 Properties of the studied materials

Material	ρ_0 g/cc	c_1 km/s	c_s km/s	c_b km/s	E' GPa	G GPa	B GPa	E GPa	ν	σ_{sp} GPa
Sintered Al10SiMg	2.67 ^a	6.78 (2)	3.32 (1)	5.60 (3)	123 (1)	29.5 (3)	83.5 (4)	79.0 (4)	0.342 (3)	0.99 (2)
RBBC	2.44	12.53 (3)	7.63 (2)	8.91 (4)	383 (2)	142 (1)	194 (2)	342 (2)	0.206 (5)	0.42 (2)
Alumina	3.94	10.86 (3)	6.40 (2)	7.96 (4)	465 (3)	161 (2)	250 (3)	398 (3)	0.234 (5)	1.50 (3)

^aRelative uncertainty of the density determination is negligibly small with respect to the uncertainties of other measured properties in parentheses (last digit)

of the pullback measurements and discussed in the “Determination of the spall strengths of the constituents” section.

All of the impact tests conducted in the present study were performed with a 6-m-long, 25 mm smooth bore gas gun equipped with an optic fiber system for accurate determination of impact velocity. The sample holder adjacent to the gun muzzle provides an impactor-sample misalignment of about 0.5 mrad. This is especially important for tests performed with relatively low impact velocities, as conducted here. In all impact tests, either velocity of the rear sample surface or that of the sample-window interface (for tests with ceramics) was continuously monitored by VISAR with an interferometric constant 96.4 m/s per fringe.

Although the strengths of the joints between ceramics and metals were unknown, it was plausible to assume that they were not too high. Accordingly, all tests were performed with relatively low impact velocity. At the same time, taking into account the relatively high spall strength of the SPS-processed alumina [11] and of the metallic constituent [15], spall-oriented experiments with these materials were performed at higher (175–190 m/s) impact velocities.

For measuring the spall strength of an Al10SiMg sample of approximately 2 mm thickness, the sample was shock-loaded with a 0.5 mm copper impactor accelerated to a velocity of about 190 m/s. The history of velocity of the rear surface of this sample is shown in Fig. 4a. In tests with ceramic constituents, the rear surfaces of RBBC and alumina samples were backed by a 5.1 mm-thick polymethylmetacrylate

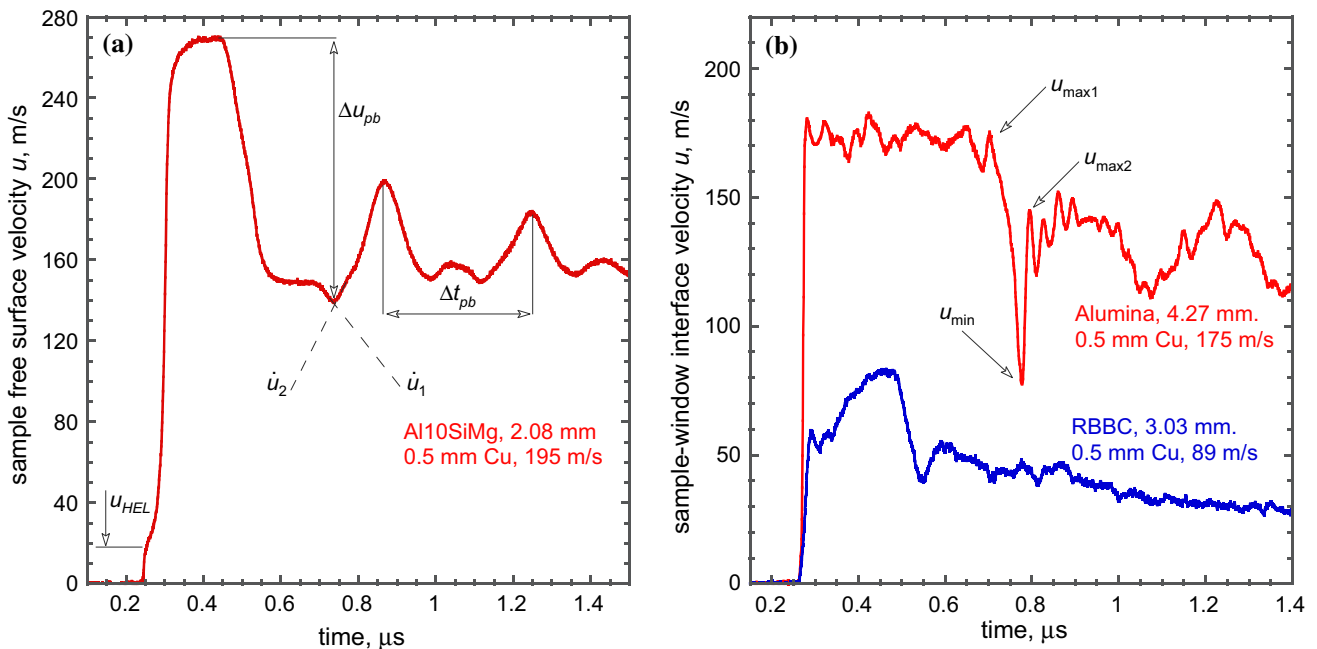


Figure 4 Free surface velocity histories of the metallic (a) and ceramic (b) constituents of metal–ceramic joints. The tests parameters are shown next to the waveforms. Arrows marks the parameters used for calculating σ_{HEL} , Y and σ_{sp} .

(PMMA) window whose shock properties were taken from [16]. In these tests, the velocity monitored by VISAR was that of the sample-window interface. The corresponding velocity histories are shown in Fig. 4b.

The stress at the Hugoniot elastic limit (HEL) of Al10SiMg, calculated as $\sigma_{\text{HEL}} = \rho_0 c_1 u_{\text{HEL}}/2$ [17], is equal to $\sigma_{\text{HEL}} = 0.13 \pm 0.01$ GPa. The yield strength $Y = 2G\sigma_{\text{HEL}}/E'$ [17], corresponding to uniaxial stress loading, is equal to 63 ± 5 MPa. The spall strength of the Al10SiMg alloy was determined using the expression:

$$\sigma_{\text{sp}} = \frac{1}{2} \rho_0 c_b (\Delta u_{\text{pb}} + \delta u), \quad (1)$$

where c_b is the bulk speed of sound, and $\delta u = h_{\text{sp}}(1/c_b - 1/c_l)|\dot{u}_1|u_2/(|\dot{u}_1| + u_2)$ is a correction for distortion of the waveform as a result of the different propagation velocities of the spall signal front and of the rarefaction wave ahead of it in the elastic–plastic medium [18]. The value of σ_{sp} , estimated using Eq. (1), is given in the rightmost column of Table 1. It should be, however, noted that for this test, the correction δu was found to be smaller than $0.03\Delta u_{\text{pb}}$, suggesting that instead of Eq. (1), a simplified expression:

$$\sigma_{\text{sp}} = \frac{1}{2} \rho_0 c_b \Delta u_{\text{pb}}, \quad (1a)$$

may be used for estimating σ_{sp} of the metallic constituent.

Since the spall strength of the ceramic constituents was determined in the impact experiments with window backing of the sample, the value of their spall strength can be estimated either using $u_{\text{max}1}$ and u_{min} (as in Fig. 4b) in:

$$\sigma_{\text{sp}} = \frac{1}{2} [Z_{\text{cer}}(u_{\text{max}1} - u_{\text{min}}) - (Z_{\text{PMMA}}^L u_{\text{max}1} + Z_{\text{PMMA}}^U u_{\text{min}})], \quad (2a)$$

or using u_{min} and $u_{\text{max}2}$ in:

$$\sigma_{\text{sp}} = \frac{1}{2} [Z_{\text{cer}}(u_{\text{max}2} - u_{\text{min}}) + Z_{\text{PMMA}}^R u_{\text{max}2} - Z_{\text{PMMA}}^U u_{\text{min}}], \quad (2b)$$

where $Z_{\text{cer}} = \rho_{0\text{cer}} c_{l\text{cer}}$ is the acoustic impedance of the ceramic, and $Z_{\text{PMMA}}^L, Z_{\text{PMMA}}^U$ and Z_{PMMA}^R are the PMMA impedances corresponding, respectively, to the loading from the initial state to that state of $u_{\text{max}1}$, unloading from $u_{\text{max}1}$ to u_{min} , and reloading from u_{min} to $u_{\text{max}2}$ [11]. The two equations, 2a and 2b, should be, respectively, used for weak and moderate impact

testing, give the similar figures for σ_{sp} of the ceramics studied. The corresponding positions in the rightmost column of Table 1 list the averages of the two.

Determination of the joint strength between aluminum alloys and RBBC composites

The strength of the joint was studied on a sandwich-like sample of approximately 20 mm diameter containing a plane-parallel RBBC ceramic part of ~ 3 mm thickness and a plane-parallel Al10SiMg part of ~ 1.5 -mm thickness, joined by the SPS technique. The sandwich was impact-loaded from its ceramic side by a 1.04 mm aluminum impactor with a velocity 89.3 ± 0.6 m/s, while the velocity of the rear surface of the metal part of the sandwich was continuously monitored by VISAR with an interferometer constant of 96.4 m/s per fringe. The outcome of this test is shown in Fig. 5.

In the velocity history shown in Fig. 5, clear evidence of the spall-like failure of the shocked sample is presented. The first velocity peak, corresponding to

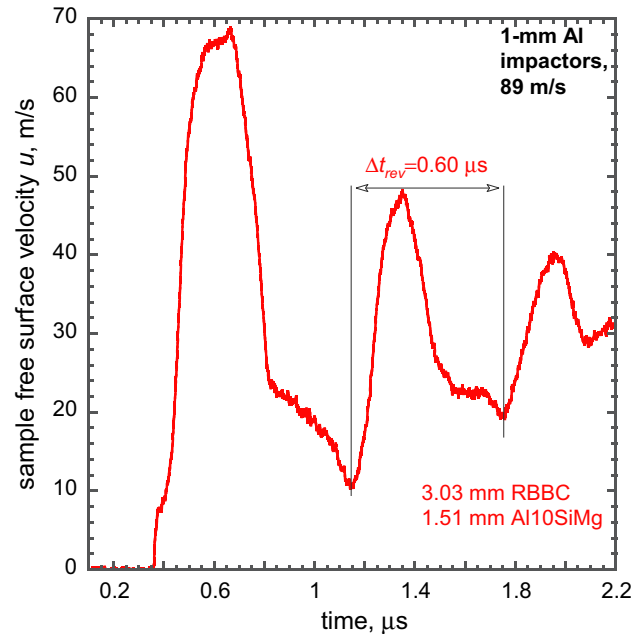


Figure 5 The velocity history recorded at the rear free surface of the metal part of a sandwich-like sample containing RBBC ceramic and Al10SiMg metal parts after a 90 m/s impact by a 1-mm aluminum impactor. The thicknesses of the parts are given next to the velocity history. The open arrow and the adjacent number mark the period of the signal reverberation Δt_{rev} in the part of the sandwich separated due to the impact.

the loading–unloading cycle of the metal part, is followed by a train of weaker peaks, corresponding to the reverberation of the residual (after spall) momentum in the spall plate. The amplitude of the compressive pulses (estimated based on mass-momentum conservation across the shock front [19]) in this test was about 0.49 ± 0.01 GPa. Accordingly, the amplitude of the tensile pulse should be close to this number, which is lower than the σ_{sp} of the Al10SiMg part and greater than the σ_{sp} of the RBBC ceramic (Table 1). In principle, a tensile pulse with such amplitude cannot produce spall fracture in the Al10SiMg part of the ceramic–metal sandwich. The fracture instead has to occur either at the joint or within the RBBC ceramic composite layer. If the fracture takes place at the sandwich joint, the period of the reverberation Δt_{rev} marked in Fig. 5, namely 0.60 s, should be equal to that of the elastic wave $\Delta t_{el} = 2\delta^{Met}/c_1^{Met}$ in the metal layer, namely 0.56 μ s. This means that for the test portrayed in Fig. 5, the fracture occurs rather within the body of the ceramic layer than at the ceramic–metal interface ($\Delta t_{rev} > \Delta t_{el}$). This also means that the dynamic tensile strength of the joint is higher than that of the ceramic part of the sandwich, i.e., the tensile strengths of the Al10SiMg joint with RBBC is greater than 0.42 GPa. Assuming that both the compressive and tensile deformations of both types of ceramic parts are elastic (the impact is weak), we can estimate the exact depth of the spall site with respect to the ceramic–metal interface by $d = (\Delta t_{rev}/2 - \Delta t_{el}/2)c_1^{Cer}$. For the joint comprising RBBC ceramic with Al10Si2 Mg, this depth is equal to $d \approx 0.2$ mm. It should be noted that in the case of the RBBC-metal joint the failure will always occur in the body of a weak ceramic layer. This allowed us to confine the testing of the RBBC-metal joint to that shown in Fig. 5. At the same time, the fractography examination of the in-ceramic failure is virtually impossible; due to the low strength of the RBBC layer the contact surface of softly recovered metal part is completely free of the remains of the joined ceramic.

Determination of the joint strength between Al10SiMg alloy and alumina

The strength of the joint between SPS-processed alumina and Al10SiMg alloy was studied in experiments similar to those discussed above. Taking into

account the relatively high tensile strength of alumina, the velocity of the 1 mm aluminum impactors in these experiments was higher than in the previous case, i.e., 155 ± 4 m/s instead of approximately 90 m/s. As above, the tested samples were sandwich-like bi-layers containing plane parallel 4 mm-thick alumina disks of 20 mm diameter coupled with Al10SiMg layers of 1.36 and 1.67 mm thickness.

The velocity histories recorded in planar impact tests of alumina-metal joints are shown in Fig. 6. Generally, the waveforms recorded in these tests are similar to that of the RBBC-metal test although few differences are apparent. First, the velocity history obtained with the alumina-Al10SiMg pair was unusual for impact studies of segments with negative free surface velocity, which can be considered as an indication of substantial strength of the joint. Specifically, the forward-moving Al10SiMg part was dragged back prior to failure. Secondly, in the case of the alumina-Al10SiMg joint, the velocity pullback Δu , responsible for the strength of the sandwich-like sample under tension, is much greater than in the

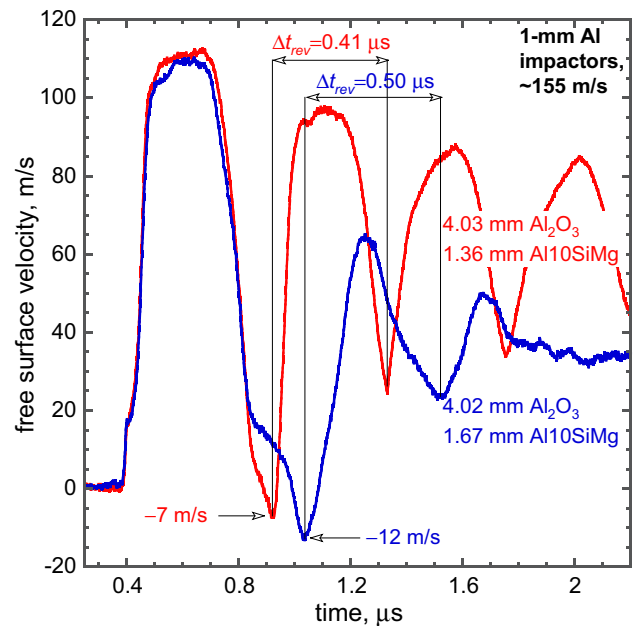


Figure 6 Velocity histories recorded at the rear free surface of the metal part of sandwich-like samples containing alumina (Al_2O_3), ceramic and Al10SiMg parts after their loading by 1 mm aluminum impactors at a velocity of about 155 m/s. The thicknesses of the parts are given next to the corresponding velocity histories. The arrows with adjacent numbers show the periods of the signal reverberations in those parts of the sandwiches separated due to the impact.

case of the joint between the RBBC composite and Al10SiMg.

The reverberation periods marked in Fig. 6 Δt_{rev} are equal to 0.41 and 0.50 μs for the tests with 1.36 and 1.67 mm-thick Al10SiMg layers, respectively. Corresponding periods of reverberation of the elastic waves $\Delta t_{\text{el}} = 2\delta^{\text{Met}}/c_1^{\text{Met}}$ in these Al10SiMg layers of the thicknesses are 0.40 and 0.49 μs , respectively. The closeness of the corresponding Δt_{rev} and Δt_{el} values, within the uncertainty of their experimental determination, suggests that the failure of alumina-Al10SiMg sandwiches occurs either exactly at the ceramic-metal interface or in its very close vicinity. Postmortem fractography of a sample softly recovered after such a test confirmed this suggestion. The failure surface shown in Fig. 7a consists of a few open voids and multiple dimples, characteristic of tensile fracture of a ductile metal, while at the bottom parts of the dimples (Fig. 7b), agglomerations of the sub-micron alumina grains still in contact with metal part of the fractured sample are seen. Unfortunately, the brittleness of the ceramic part of the joint makes virtually impossible the fractography examination of the ceramic part of the joint separated due to the impact-generated tensile stress. While the inherent plasticity helps to recover the metal part of the joint the state of the ceramic part becomes completely comminuted by reverberating compressive and release pulses. These multiple fractures are not related to the tensile fracture of the joint making the fractography of the ceramic part of little help.

Applying Eq. (1) to the velocity histories shown in Fig. 6 yields values of the joints tensile strength equal to $\sigma_{\text{Al10SiMg-Al}_2\text{O}_3} = 0.94 \pm 0.05 \text{ GPa}$ and $\sigma_{\text{Al10SiMg-Al}_2\text{O}_3} = 0.97 \pm 0.05 \text{ GPa}$ for the tests with the 1.67 and 1.36 mm-thick Al10SiMg layers, respectively. The measured values of the strength of the two joints, 0.94 ± 0.05 and $0.97 \pm 0.05 \text{ GPa}$, are found to be extremely close. Since it is hardly possible to suggest any departure from the employed joining technology capable of substantial changing of the strength of the joint the closeness of the two values allows one to conclude that in the case of alumina-metal joining the results are reasonably reproducible.

Quantitatively, the obtained numbers are only slightly lower than the separately determined spall strength of Al10SiMg, where $\sigma_{\text{spall Al10SiMg}} = 0.99 \pm 0.02 \text{ GPa}$ (Table 1). As such, the tensile pulse generated within the metal layer does not appear on the recorded waveforms of a spall-like signature (with the exception of some decrease in sample free surface deceleration) related to the incipient damage within the layer. Due to the closeness of the tensile pulse fracturing the joint to the spall strength of the corresponding metal part, one can expect, at the least, initiation of tensile failure at a distance from the part free surface approximately equal to the impactor thickness (1 mm). Such failure initiation should result in the appearance of an acceleration signature at the recorded waveform. The presence of such a signature at the waveform recorded with the sandwich sample containing 4.02 mm Al_2O_3 and 1.67 mm Al10SiMg layers is confirmed by metallographic examination of the cross section of the Al10SiMg part of the sample,

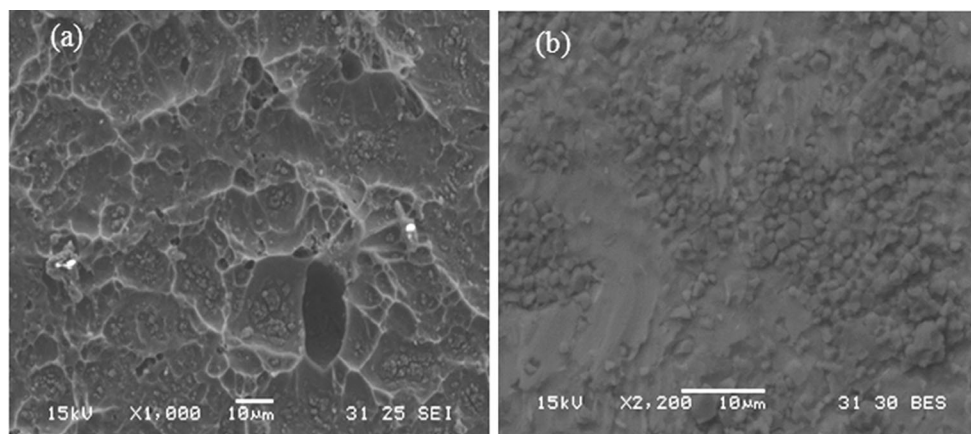


Figure 7 Fracture surface of a sample made of 4.02 mm-thick alumina layer and a 1.67 mm-thick layer of Al10SiMg. The bottoms of the dimples (a, $\times 1000$) are covered by residual alumina

grains (b, $\times 2200$) still in contact with the metal, typical of viscous tensile fracture of metals.

softly recovered after this test (Fig. 8). The tensile fracture starts at the to-be spall site located at a distance of about 1 mm (thickness of the impactor) from the free surface of the Al10SiMg layer. The dynamic tensile (spall) fracture is a sequence of void nucleation, the growth and, ultimately, coalescence [18] with creation of two new surfaces. Keeping this in mind, Fig. 8 allows one to assume that the tensile pulse duration at the to-be spall site is sufficient for void nucleation and their growth up to several tens of microns yet still insufficient for the void coalescence that results in the creation of the spall plane.

The results of the measurements of the strength of the joint between alumina and the aluminum alloy lead to two questions: (1) why did the strength of the joint virtually coincides with the spall strength of the metal part? and (2) why did the fracture occur at the joint, yet not at the to-be spall plane?

The answer to the both questions can be found with the help of recent atomistic simulations of the structure of the aluminum–alumina interface [20]. According to these simulations, the Al/Al₂O₃ interface represents almost coherent regular triangle domains of Al^(Al)–Al^(Al)–Al^(Al₂O₃) atoms in an ABC sequence, characteristic of an FCC aluminum lattice alternated with triangles of stacking faults (SF) with the ABAB sequence of aluminum atoms characteristic of HCP lattice. Since the inter-atomic forces at the interface and in the bulk material are virtually equal (the first and second coordination spheres of FCC and HCP coincide; a difference only appears in the third sphere), the tensile stress required for breaking

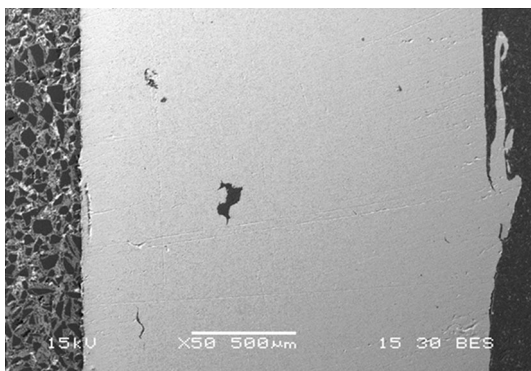


Figure 8 Metallographic cross section of the metallic part of the Al₂O₃–Al10SiMg sandwich initially containing 4.02 mm Al₂O₃ and 1.67 mm metallic layers. The tensile-generated void visible at to-be spall plane (~ 1 mm from the free, right, surface of Al10SiMg layer) did not grow enough to create two new surfaces.

the inter-atomic bonds either at the joint interface or in the bulk material are virtually equal. At the same time, the nucleation of voids giving rise to the spall process and the subsequent void growth, are strongly favored by the presence of stacking faults [21] which are virtually absent in the bulk aluminum due to the high (~ 0.2 J/m²) stacking fault energy of aluminum [22]. One can thus assume that spallation, although triggered by the same tensile stress as in the bulk material, proceeds much faster at the ceramic metal interface and leads to joint fracture.

Conclusions

Joints between dissimilar materials, namely between alumina and reaction-bonded boron carbides and Al10SiMg alloy, were produced using spark plasma sintering (SPS) and then tested in a series of planar impact experiments designed to measure the dynamic tensile (spall) strength of the joint. The second part of the work served to verify a general technique for testing the strength of the bond between two materials when stuck together. Such measurements showed that the dynamic tensile strength of the joint region between a reaction-bonded boron carbide composite and Al10SiMg alloy exceeds that of the composite, with the fracture of the shock-loaded ceramic–metal sandwich evidently taking place in the composite part (about 0.2 mm away from the interface).

This was not the case for the joint of alumina with the Al10SiMg alloy. The dynamic tensile strength of this interface virtually coincided with that of the metal parts, while the tensile fracture occurred exactly at the interface and not within the bulk of the metal, despite of the fact that the tensile pulse of the amplitude was sufficient for fracture within the metal part (about 0.5 mm away from the interface). The recently published results of atomistic calculations of the structure of the alumina–aluminum interface explain this surprising fact.

Acknowledgements

Financial support by the Israeli Ministry of Defense to Prof. E. Zaretsky (Grant 87576411) and to Prof. N. Frage (Grant 87541011) is gratefully acknowledged.

References

- [1] Howe JM (1993) Bonding, structure and properties of metal/ceramic interfaces. *Mater Res Symp Proc* 314:27–37
- [2] Lemus-Ruiz J, Aguilar-Reyes EA (2004) Mechanical properties of silicon nitride joints using a Ti-foil interlayer. *Mater Lett* 58(19):2340–2344
- [3] Centeno A, Rocha VG, Borrell A, Blanco C, Fernandez A (2012) Fabrication of C/SiC composites by combining liquid infiltration process and spark plasma sintering technique. *Ceram Int* 38:2171–2175
- [4] Guillard F, Allemand A, Lulewicz J-D, Galy J (2007) Densification of SiC by SPS—effects of time, temperature and pressure. *J Eur Ceram Soc* 27:2725–2728
- [5] Luo Y, Li S, Pan W, Li L (2004) Fabrication and mechanical evaluation of SiC–TiC nanocomposites by SPS. *Mater Lett* 58:150–153
- [6] Liu W, Naka M (2003) In situ joining of dissimilar nanocrystalline materials by spark plasma sintering. *Scripta Mater* 48:1225–1230
- [7] Rizzo S, Grasso S, Salvo M, Casalegno V, Reece MJ, Ferraris M (2014) Joining of C/SiC composites by spark plasma sintering technique. *J Eur Ceram Soc* 34:903–913
- [8] Miriyev A, Barlam D, Shneck R, Stern A, Frage N (2014) Steel to titanium solid state joining displaying superior mechanical properties. *J Mater Process Technol* 214:2884–2890
- [9] Miriyev A, Stern A, Tuval E, Kalabukhov S, Hooper Z, Frage N (2013) Titanium to steel joining by spark plasma sintering (SPS) technology. *J Mater Process Technol* 213:161–166
- [10] Baumung K, Kanel GI, Müller G, Singer J (2000) Measurement of the adhesive strength of 200 μm thick turbine blade coatings by a dynamic method, shock compression of condensed matter—1999. *AIP* 505:1207–1210. <https://doi.org/10.1063/1.1303678>
- [11] Gurlitsky I, Zaretsky E, Kalabukhov S, Dariel MP, Frage N (2014) Dynamic compressive and tensile strengths of spark plasma sintered alumina. *J Appl Phys* 115:243505. <https://doi.org/10.1063/1.4885436>
- [12] Hayun S, Weizmann A, Dariel MP, Frage N (2009) The effect of particle size distribution on the microstructure and the mechanical properties of boron carbide-based reaction-bonded composites. *Int J Appl Ceram Technol* 6(4):492–500
- [13] Barker LM, Hollenbach RE (1972) Laser interferometer for measuring high velocities of any reflecting surface. *J Appl Phys* 43:4669–4775
- [14] Kanel GI (2010) Spall fracture: methodological aspects, mechanisms and governing factors. *Int J Fract* 163:173–191. <https://doi.org/10.1007/s10704-009-9438-0>
- [15] Chen X, Asay JR, Dwivedi SK, Field DP (2006) Spall behavior of aluminum with varying microstructures. *J Appl Phys* 99:023528
- [16] Barker LM, Hollenbach RE (1970) Shock-wave studies of PMMA, fused silica, and sapphire. *J Appl Phys* 41:4208–4226. <https://doi.org/10.1063/1.1658439>
- [17] Kanel GI, Razorenov SV, Fortov VE (2004) Shock-wave phenomena and the properties of condensed matter. Springer, New York, p 33
- [18] Antoun T, Seaman L, Curran D, Kanel GI, Razorenov SV, Utkin AV (2002) Spall fracture. Springer, New-York, Berlin, Heidelberg, p 90, 99
- [19] Duvall GE, Graham RA (1977) Phase transitions under shock-wave loading. *Rev Mod Phys* 49(3):523–577
- [20] Pilania G, Thijsse BJ, Hoagland RG, Lazić I, Valone SM, Liu X-Y (2014) Revisiting the Al/Al₂O₃ interface: coherent interfaces and misfit accommodation. *Sci Rep* 4:4485. <https://doi.org/10.1038/srep04485>
- [21] Zaretsky E (1995) Dislocation multiplication behind the shock front. *J Appl Phys* 78:3740. <https://doi.org/10.1063/1.359954>
- [22] Gallagher PCJ (1970) The influence of alloying, temperature, and related effects on the stacking fault energy. *Metall Trans* 1(9):2429–2461